2013

Simulation of Mono- and Bidisperse Gas-Particle Flow in a Riser with a Third-Order Quadrature-Based Moment Method

Alberto Passalacqua
Iowa State University, albertop@iastate.edu

Rodney O. Fox
Iowa State University, rofox@iastate.edu

I&EC research
Industrial & Engineering Chemistry Research

Article

pubs.acs.org/IECR

Simulation of Mono- and Bidisperse Gas-Particle Flow in a Riser with a Third-Order Quadrature-Based Moment Method

Alberto Passalacqua* and R. O. Fox*

Department of Chemical and Biological Engineering, 2114 Sweeney Hall, Iowa State University, Ames, Iowa 50011-2230, United States

ABSTRACT: Gas-particle flows can be described by a kinetic equation for the particle phase coupled with the Navier−Stokes equations for the fluid phase through a momentum exchange term. The direct solution of the kinetic equation is prohibitive for most applications due to the high dimensionality of the space of independent variables. A viable alternative is represented by moment methods, where moments of the velocity distribution function are transported in space and time. In this work, a fully coupled third-order, quadrature-based moment method is applied to the simulation of mono- and bidisperse gas-particle flows in the riser of a circulating fluidized bed. Gaussian quadrature formulas are used to model the unclosed terms in the moment transport equations. A Bhatnagar−Gross−Krook (BGK) collision model is used in the monodisperse case, while the full Boltzmann integral is adopted in the bidisperse case. The predicted values of mean local phase velocities, rms velocities, and particle volume fractions are compared with the Euler−Lagrange simulations and experimental data from the literature. The local values of the time-average Stokes, Mach, and Knudsen numbers predicted by the simulation are reported and analyzed to justify the adoption of high-order moment methods as opposed to models based on hydrodynamic closures.

INTRODUCTION

Gas-particle flows in risers have been the topic of extensive research in order to develop reliable computational models capable of describing their features. In general, two kinds of approaches are possible to describe the particle phase: a Lagrangian approach, where each particle trajectory is resolved independently, applying the fundamental laws of Mechanics; and an Eulerian approach, in which the particle phase is described by transport equations for moments of the particle velocity distribution function. The computational convenience and the absence of statistical noise characteristic of Eulerian models make them very attractive both for research and applications, and significant effort to improve their formulation has been spent in the last two decades. Nevertheless, when properly formulated,[1] the predictions from Lagrangian and Eulerian models for the particle phase should be identical.

Hydrodynamic models for circulating-fluidized-bed (CFB) reactors have been developed[2,3] to account for heat transfer and to introduce a normal stress modulus for the particle phase. By adopting an appropriate drag correlation,[4] one can properly predict flow regimes typical of CFB risers.[5,6] If all the interactions between the phases are accounted for and correlated to the averaged and fluctuating components of the phase velocity fields,[7,8] a hydrodynamic model is able to properly predict the behavior of gas−solid flow in a riser. A stationary hydrodynamic model[7] is able to predict the particle phase stresses through the kinetic theory of granular flow as a function of the particle fluctuating energy (granular energy). A modified model[9] has been proposed and validated against experimental data,[10] showing a high sensitivity to the value of the restitution coefficient, whose reduction may lead to a wrong prediction of the particle segregation patterns inside the duct. In general, such sensitivity to model parameters points to a breakdown of the hydrodynamic description for relatively dilute flows.[1]

For turbulent flow, a one-equation turbulence model[11] has been used to describe the gas-phase turbulence by adopting standard wall-functions for the zone near the wall. A zero-equation closure[12] for the gas-phase turbulence has also been proposed. Extending previous work[7] to arbitrarily inclined ducts, a model accounting for the effects of particle sliding and rotation has been developed.[13] A low Reynolds number two-equation k-ε model for the gas phase has been proposed[14] to eliminate the need for wall functions. The influence of turbulence both on the transport equations and on the kinetic theory closure equations has been studied,[15] leading to a reformulation of the dissipation term of granular energy, which resulted in a reduced sensitivity of the model to the value of the particle restitution coefficient. A CFB riser has been simulated[16,17] using the kinetic theory of granular flow, neglecting the gas-phase turbulence. A model that couples a two-equation turbulence model with a set of two equations for the particle-phase turbulent kinetic energy and for the gas-particle velocity correlation has also been proposed.[18−20] It is noteworthy that RANS turbulence models for gas-particle flows are rarely compared to Lagrangian simulations and, in fact, rely on adjustable parameters to close the interaction terms between the two phases.

Following the ideas behind large-eddy simulations (LES),[1] LES models have been introduced[12,21−24] using a standard sub-grid stress model[25] to describe the turbulence of the gas phase. Recently,[26] a Lagrangian description of the particle phase coupled to an LES model for the gas phase has been compared to a multi-fluid model of a circulating fluidized bed. For dense

Special Issue: L. T. Fan Festschrift

Received: February 16, 2012
Revised: August 30, 2012
Accepted: August 31, 2012
Published: August 31, 2012

dx.doi.org/10.1021/ie300424m | *Ind. Eng. Chem. Res.* 2013, 52, 187−198

gas-particle flows, a two-scale, second-order moment particle-phase turbulence model has been developed.[27] A novel LES approach for particle-laden turbulent flows in the framework of the Eulerian formalism for inertial particles has also been proposed.[28] Experiments in a riser with monodisperse particles have been carried out[29] and compared to the results of numerical simulations performed using the Lagrangian discrete particle model (DPM) approach coupled to an LES description of the gas phase.

In this work, we consider a monodisperse riser flow from the literature[29] and a bidisperse riser flow examined experimentally[22] and simulated[30] using the Euler−Lagrange approach. We perform numerical simulations of both systems using a third-order quadrature-based moment method coupled with a fluid solver.[31] Results are compared to experimental data and to Euler−Lagrange simulations.[29,30] Flow statistics of the particle phase are computed, and dimensionless parameters such as the particle-phase Mach, Knudsen, and Stokes numbers are examined in order to justify the adoption of high-order moment methods. Of particular interest is the closure used to describe inelastic particle−particle collisions[32] in the Eulerian model. We show in this work that closures based on the evaluation of the full Boltzmann integral are required in order to properly capture the collisional change in properties of the particulate phase in the case of bidisperse flows. In this case, linearized models, which provide satisfactory results in the monodisperse case, are unable to properly describe properties like the evolution of the temperature ratio at the homogeneous cooling state as a function of the particle diameter ratio.

The remainder of this work is organized as follows. First, we provide a brief overview of the Euler−Euler model and the quadrature-based moment methods introduced in our earlier works.[31−39] Next, we describe the simulation setup used to model the riser experiments with monodisperse[29] and bidisperse[22] particles. Finally, our simulation results are presented and qualitatively compared to the experimental data and Euler−Lagrange simulation results.[30]

MODEL DESCRIPTION

Fluid-Phase Governing Equations. The fluid phase, assumed to be incompressible and isothermal, is described by a continuity and a momentum equation as in traditional two-fluid models.[40−42] The fluid continuity equation is

$$\frac{\partial}{\partial t}(\alpha_g \rho_g) + \nabla\cdot(\alpha_g \rho_g \mathbf{U}_g) = 0 \tag{1}$$

and the fluid momentum equation is

$$\frac{\partial}{\partial t}(\alpha_g \rho_g \mathbf{U}_g) + \nabla\cdot(\alpha_g \rho_g \mathbf{U}_g \otimes \mathbf{U}_g) = \nabla\cdot(\alpha_g \tau_g) - \alpha_g \nabla p + \alpha_g \rho_g \mathbf{g} + \mathbf{M}_{gp} \tag{2}$$

where α_g, ρ_g, $\mathbf{U}_g$ are the fluid-phase volume fraction, density and mean velocity, $\mathbf{M}_{gp}$ represents the momentum exchange term due to the drag between the fluid and particle phases, and $\mathbf{g}$ is the gravitational acceleration vector. The stress tensor τ_g is

$$\tau_g = \mu_g[\nabla \mathbf{U}_g + (\nabla \mathbf{U}_g)^T] - \frac{2}{3}\mu_g(\nabla\cdot\mathbf{U}_g)\mathbf{I} \tag{3}$$

where μ_g is the viscosity of the fluid and $\mathbf{I}$ the unit tensor. The fluid-phase equations are coupled to the particle-phase description through the volume-fraction constraint $\alpha_g + \alpha_p = 1$ and the momentum exchange term. For the dilute gas-particle flows considered in this work, momentum coupling is the dominant phase-interaction term.

Particle-Phase Governing Equations. The particle phase is described in analogy to the kinetic theory of a gas composed of smooth, noncohesive spheres.[32] The governing equation of each particle type in the granular mixture is then represented by a kinetic equation for the particle number density function $f_i(t,\mathbf{x},\mathbf{v}_i)$:[43−45]

$$\frac{\partial f_i}{\partial t} + \mathbf{v}_i\cdot\nabla_{\mathbf{x}} f_i + \nabla_{\mathbf{v}_i}\cdot(\mathbf{A}_i f_i) = \mathbb{C}_{ij} \tag{4}$$

where $\mathbf{v}_i$ is the velocity vector of the ith particle type, $\mathbf{A}_i$ is the acceleration acting on each particle, including gravity and drag, and $\mathbb{C}_{i,j}$ represents the rate of change in the number density function due to binary collisions between particles of types i and j. For the dilute cases considered in this work, we can neglect the collisional flux term[32] in the kinetic equation.

Quadrature-Based Moment Method. The moments of the number density function f_i are defined, for each particle type, as

$$M_i^{\gamma}(t,\mathbf{x}) = \int_{\mathbb{R}^3} v_{i,1}^k v_{i,2}^l v_{i,3}^m f_i(t,\mathbf{x},\mathbf{v}_i)\mathrm{d}\mathbf{v}_i \tag{5}$$

where $\gamma = k + l + m$ is the order of the moment. In this work, we will use moments up to third order in the velocity[35]

$$M_i^0(t,\mathbf{x}) = \int_{\mathbb{R}^3} f_i(t,\mathbf{x},\mathbf{v}_i)\mathrm{d}\mathbf{v}_i \tag{6}$$

$$M_{i,k}^1(t,\mathbf{x}) = \int_{\mathbb{R}^3} v_{i,k} f_i(t,\mathbf{x},\mathbf{v}_i)\mathrm{d}\mathbf{v}_i \tag{7}$$

$$M_{i,kl}^2(t,\mathbf{x}) = \int_{\mathbb{R}^3} v_{i,k} v_{i,l} f_i(t,\mathbf{x},\mathbf{v}_i)\mathrm{d}\mathbf{v}_i \tag{8}$$

$$M_{i,klm}^3(t,\mathbf{x}) = \int_{\mathbb{R}^3} v_{i,k} v_{i,l} v_{i,m} f_i(t,\mathbf{x},\mathbf{v}_i)\mathrm{d}\mathbf{v}_i \tag{9}$$

which we denote by the moment vector $\mathbf{M}_i^{\gamma}$. By construction, the zero-order moment for each particle type is equal to the particle-phase volume fraction, i.e., $M_i^0 = \alpha_{p,i}$.

Using the moment definition, transport equations for the moments of f_i can be found from eq 4, leading to

$$\frac{\partial \mathbf{M}_i^{\gamma}}{\partial t} + \nabla_{\mathbf{x}}\cdot\mathbf{M}_i^{\gamma+1} = \mathbf{A}_i^{\gamma} + \mathbf{C}_{ij}^{\gamma} \tag{10}$$

where $\mathbf{A}_i^{\gamma}$ and $\mathbf{C}_{ij}^{\gamma}$ are, respectively, the moments of order γ of the acceleration term and of the collision term. It is worth noticing that the coupling between each particle type and the fluid phase is achieved by means of the acceleration term,[31] while the momentum exchange between particles is described by the collision term. As a consequence, the set of equations constituted by the Navier−Stokes equations for the fluid and the moment transport equations for each particle type accounts for the full coupling among the phases, without any need to specify a drag correlation for particle−particle interactions between particle types.

In this work, each particle type is described considering 20 moments of f_i, up to the third order.[35] As a consequence, 20 transport equations for the moments are solved for each type of particle considered (i.e., one type for monodisperse and two types for bidisperse). Such equations, however, are unclosed because they depend on the spatial fluxes of higher-order moments, the acceleration term and on the collision term.

dx.doi.org/10.1021/ie300424m | Ind. Eng. Chem. Res. 2013, 52, 187−198

Gaussian quadrature formulas are used to provide closures for these terms as a function of a set of weights n_α and abscissas $\mathbf{U}_\alpha$. Weights and abscissas are computed from the set of transported moments by means of an inversion algorithm. In this work, a set of eight weights and abscissas per each velocity component is used.[35] However, higher-order quadrature formulas are also possible.[36,39]

The moments can be computed as a function of the quadrature weights and abscissas using the definition in eq 5, where we drop the index representing the particle type because the formulas are identical for each type:

$$M^0 = \sum_{\alpha=1}^{\beta} n_\alpha,\ M_k^1 = \sum_{\alpha=1}^{\beta} n_\alpha U_{\alpha k},$$
$$M_{kl}^2 = \sum_{\alpha=1}^{\beta} n_\alpha U_{\alpha k} U_{\alpha l},\ M_{klm}^3 = \sum_{\alpha=1}^{\beta} n_\alpha U_{\alpha k} U_{\alpha l} U_{\alpha m} \tag{11}$$

The source terms due to drag exerted by the fluid and gravity are computed as

$$A_k^1 = \sum_{\alpha=1}^{\beta} n_\alpha \left(\frac{F_{k\alpha}^{\mathrm{D}}}{m_{\mathrm{p}}} + g_k \right),$$
$$A_{kl}^2 = \sum_{\alpha=1}^{\beta} n_\alpha \left[\left(\frac{F_{k\alpha}^{\mathrm{D}}}{m_{\mathrm{p}}} + g_k \right) U_{l\alpha} + \left(\frac{F_{l\alpha}^{\mathrm{D}}}{m_{\mathrm{p}}} + g_l \right) U_{k\alpha} \right],$$
$$A_{klm}^3 = \sum_{\alpha=1}^{\beta} n_\alpha \left[\left(\frac{F_{k\alpha}^{\mathrm{D}}}{m_{\mathrm{p}}} + g_k \right) U_{l\alpha} U_{m\alpha} + \left(\frac{F_{l\alpha}^{\mathrm{D}}}{m_{\mathrm{p}}} + g_l \right) U_{m\alpha} U_{k\alpha} + \left(\frac{F_{m\alpha}^{\mathrm{D}}}{m_{\mathrm{p}}} + g_m \right) U_{k\alpha} U_{l\alpha} \right] \tag{12}$$

The drag force terms are given by

$$\mathbf{F}_\alpha^{\mathrm{D}} = \frac{m_{\mathrm{p}}}{\tau_\alpha^{\mathrm{D}}} (\mathbf{U}_{\mathrm{g}} - \mathbf{U}_\alpha) = K_{\mathrm{gp},\alpha} (\mathbf{U}_{\mathrm{g}} - \mathbf{U}_\alpha) \tag{13}$$

where m_{p} is the particle mass. The drag time, computed for each velocity abscissa, is calculated as

$$\tau_\alpha^{\mathrm{D}} = \frac{4 d_{\mathrm{p}}^2 \rho_{\mathrm{p}}}{3 \alpha_{\mathrm{g}} \mu_{\mathrm{g}} C_{\mathrm{D}}(\mathrm{Re}_{\mathrm{p}\alpha}, \alpha_{\mathrm{g}}) \mathrm{Re}_{\mathrm{p}\alpha}} \tag{14}$$

where ρ_{p} is the material density of the solid, and d_{p} is particle diameter. The particle Reynolds number is defined for each abscissa by

$$\mathrm{Re}_{\mathrm{p}\alpha} = \frac{\rho_{\mathrm{g}} d_{\mathrm{p}} |\mathbf{U}_{\mathrm{g}} - \mathbf{U}_\alpha|}{\mu_{\mathrm{g}}} \tag{15}$$

and the drag coefficient C_D is modeled as[4]

$$C_{\mathrm{D}}(\mathrm{Re}_{\mathrm{p}}, \alpha_{\mathrm{g}}) = \frac{24}{\alpha_{\mathrm{g}} \mathrm{Re}_{\mathrm{p}}} [1 + 0.15 (\alpha_{\mathrm{g}} \mathrm{Re}_{\mathrm{p}})^{0.687}] \alpha_{\mathrm{g}}^{-2.65} \tag{16}$$

The moment spatial fluxes are represented by the second term on the left-hand side of eq 10 and are computed according to their kinetic definition[34−36] in order to ensure the realizability of the set of moments. Details of the implementation of kinetic spatial fluxes with high-order realizable schemes are available elsewhere.[38]

As noted in the Introduction, the principal difference between the Euler−Lagrange and the Euler−Euler model described above is the treatment of the collision term. In the discrete particle model used in the Lagrangian simulations[30] of the particle phase, the hard-sphere collisions are computed exactly. In contrast, in the kinetic equation the hard-sphere collisions are approximated using the Boltzmann collision integral, which invokes a closure concerning the particle pair correlation.[44,47,48] Thus, all else being equal (e.g., the treatment of the drag force), the accuracy of the collision model in capturing the dependence of the lower-order moments on hard-sphere collisions will be the main source of differences between the two modeling approaches.

Collision Model for Monodisperse Case. The collision term $\mathbb{C}$ is modeled, in the case of monodisperse particles, using the Bhatnagar−Gross−Krook (BGK) collision operator.[49] The BGK's explicit form allows its moments to be found analytically, reducing the total computational cost, without significantly affecting the accuracy of the predicted low-order moments of the velocity distribution function.[37] The expression used in this work represents an inelastic extension[37] of the ellipsoidal-statistic BGK[50]

$$\mathbb{C} = \frac{1}{\tau_c} (f_{\mathrm{es}} - f) \tag{17}$$

where τ_c is the collision time. The equilibrium distribution function f_{es} is extended from the usual Maxwellian form to account for inelastic collisions

$$f_{\mathrm{es}} = \frac{M^0}{[\det(2\pi\lambda)]^{1/2}} \exp\left[-\frac{1}{2} (v_i - U_{\mathrm{p},i}) \lambda^{-1} (v_j - U_{\mathrm{p},j}) \right] \tag{18}$$

where λ^{-1} is the inverse of the matrix λ, defined by

$$\lambda = \gamma \omega^2 \Theta_{\mathrm{p}} \mathbf{I} + (\gamma\omega^2 - 2\gamma\omega + 1)\sigma \tag{19}$$

with $\gamma = 1/\mathrm{Pr}$, $\omega = (1+e)/2$, M^0 the number density of particles (zero-order moment), $\mathbf{U}_{\mathrm{p}}$ the mean particle velocity, e the restitution coefficient, Θ_{p} the granular temperature, and σ the particle velocity covariance matrix. In this work, $\gamma = 1$, so that Pr = 1 in the standard BGK model.[45]

The non-zero source terms in the moment transport equations up to third order due to collisions are given by

$$C_{kl}^2 = \frac{\alpha_{\mathrm{p}}}{\tau_{\mathrm{c}}} (\lambda_{kl} - \sigma_{kl}),\ C_{klm}^3 = \frac{1}{\tau_{\mathrm{c}}} (\Delta_{klm} - M_{klm}^3) \tag{20}$$

where λ_{kl} and Δ_{klm} are, respectively, the second- and third-order moments of the equilibrium distribution function. The collision time τ_c is defined by

$$\tau_{\mathrm{c}} = \frac{\pi^{1/2} \gamma d_{\mathrm{p}}}{12 \alpha_{\mathrm{p}} g_0 \Theta_{\mathrm{p}}^{1/2}} \tag{21}$$

with granular temperature Θ_{p} defined in terms of the moments by

$$\Theta_{\mathrm{p}} = \frac{1}{3} (\sigma_{11} + \sigma_{22} + \sigma_{33}) \tag{22}$$

and

dx.doi.org/10.1021/ie300424m | Ind. Eng. Chem. Res. 2013, 52, 187−198

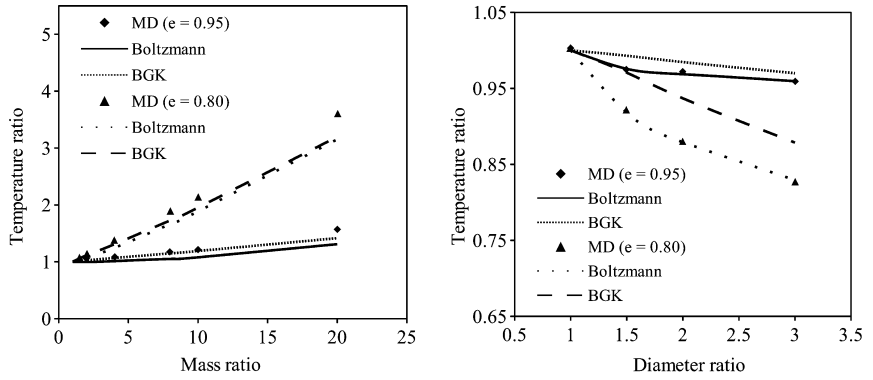

(a) Temperature ratio vs. particle mass ratio (b) Temperature ratio vs. particle diameter ratio

Figure 1. Comparison of collision models with MD simulations[54] for bidisperse granular cooling.

$$\sigma_{11} = \frac{M_{11}^2}{M^0} - \left(\frac{M_1^1}{M^0}\right)^2, \quad \sigma_{22} = \frac{M_{22}^2}{M^0} - \left(\frac{M_2^1}{M^0}\right)^2,$$
$$\sigma_{33} = \frac{M_{33}^2}{M^0} - \left(\frac{M_3^1}{M^0}\right)^2 \tag{23}$$

The radial distribution function g_0 used in this work is[51]

$$g_0 = \frac{1}{1-\alpha_p} + \frac{3\alpha_p}{2(1-\alpha_p)^2} + \frac{\alpha_p^2}{2(1-\alpha_p)^3} \tag{24}$$

and is valid for dilute and moderately dense flows with particle volume fractions below 0.55.[52] Both of the test cases studied in this work have local volume fractions well below this limit.

Collision Model for Bidisperse Case. In the case of bidisperse particles, the full hard-sphere Boltzmann collision model is used with the moment source terms derived in our previous work.[32] As discussed below, the motivation for this choice is found in the accuracy of the collision model in representing the features of polydisperse mixtures, which cannot be properly captured by linearized models. The Boltzmann collision integral for a polydisperse mixture with constant restitution coefficient e_{ij} for collisions between particle types i and j can be written as[44,47,48]

$$\mathbb{C}_{ij} = \sum_j \int\int [e_{ij}^{-2} f(t, \mathbf{x}, \mathbf{v}_i') f(t, \mathbf{x}, \mathbf{v}_j') - f(t, \mathbf{x}, \mathbf{v}_i) f(t, \mathbf{x}, \mathbf{v}_j)] B_{ij} \mathrm{d}\sigma \mathrm{d}\mathbf{v}_j$$

where the primed velocities represent the post-collisional velocities, and B_{ij} is related to the collision cross section. The source term for the moment of order $\gamma = l_1 + l_2 + l_3$ for the i-th species can be written in terms of quadrature weights and abscissas as[32]

$$C_{i,l_1l_2l_3} = \frac{6\rho_i g_{0,ij} \chi_{ij}^2}{d_{p,j}} \sum_{k_1=1}^{\beta} \sum_{k_2=1}^{\beta} n_{k_1} n_{k_2} g_{k_1k_2} I_{l_1l_2l_3}^{(0)} \tag{25}$$

where $\chi_{ij} = (d_{p,i} + d_{p,j})/(2d_{p,j})$ and $g_{k_1k_2} = |\mathbf{U}_{k_1} - \mathbf{U}_{k_2}|$ is the relative velocity for the abscissas of the two particles taking part in the collision. The analytical expressions for the terms $I_{l_1l_2l_3}^{(0)}$, corresponding to the 20 moments under consideration, are found by integrating over the collision cross section as reported elsewhere.[32] Note that eq 25 depends on the particle type through the material density ρ_i and the diameters $d_{p,i}$ and $d_{p,j}$. The radial distribution function ($g_{0,ij}$) in the bidisperse cases considered in this work is set to unity because the finite-size effects of the particles are assumed to be negligible due to the relatively low average particle volume fraction in the system (5%). A description of the full Boltzmann–Enskog integral for denser flows can be found elsewhere.[32] It is worth noticing that the quadrature-based moment closure for the collision integral described above includes all the terms in the polydisperse kinetic theory discussed in Chao et al.[53] In particular, the term corresponding to the *fluid dynamic velocity difference* is accounted for exactly in eq 25, up to the accuracy of the quadrature approximation.

The adoption of the Boltzmann collision operator, rather than of a linearized model for the collision term, is justified by comparing results obtained with molecular dynamics (MD),[54] a linearized BGK-like model,[55] and the full Boltzmann collision model in eq 25. A cooling mixture constituted by two granular species, respectively, with particle masses m_1 and m_2, particle diameters $d_{p,1}$ and $d_{p,2}$, and species volume fractions $\alpha_{p,1}$ and $\alpha_{p,2}$ was simulated for a homogeneous system using the methods reported in our previous work.[37] The ratio of the species volume fractions was assumed to be unity ($\alpha_{p,1}/\alpha_{p,2} = 1$), and the total volume fraction is $\alpha_{p,1} + \alpha_{p,2} = 0.1$. Two different values of the restitution coefficient, $e = 0.95$ and $e = 0.8$, were considered, and the results comparing the two collision models to the MD predictions are shown in Figure 1. For varying mass ratio, the particle diameters are equal; for varying diameter ratio, the particle masses are equal. When the diameter ratio is varied, both the material densities ρ_1 and ρ_2 as well as the number concentrations n_1 and n_2 must be varied to keep the species volume fractions equal.[56]

The granular mixture tends to evolve toward a homogeneous cooling state where the temperature ratio of the two species reaches a constant value, even though the individual values of the temperatures continue to decrease.[54] The value of the temperature ratio predicted by MD simulation and by QMOM with the two collision models is shown as a function of the particle mass ratio (Figure 1a) and of the particle diameter (Figure 1b). Both the BGK-like model and the Boltzmann collision model are capable of predicting the dependency of the temperature ratio as a function of the particle mass ratio. However, as illustrated in Figure 1b, the BGK-like collision model does not satisfactorily predict the dependency of the species temperature ratio on the particle size ratio, while eq 25 provides good agreement with the

dx.doi.org/10.1021/ie300424m | Ind. Eng. Chem. Res. 2013, 52, 187–198

MD predictions. Because the diameter ratio is an important parameter for the bidisperse riser flow, we use eq 25 in the remainder of this work.

Boundary Conditions. Boundary conditions for the moment transport equations are specified in terms of the quadrature approximation, as shown elsewhere.[31,35] For example, a specular reflective condition at the walls is defined as

$$\begin{pmatrix} n_\alpha \\ U_{\alpha 1} \\ U_{\alpha 2} \\ U_{\alpha 3} \end{pmatrix}_{i=0} = \begin{pmatrix} n_\alpha / e_w \\ U_{\alpha 1} \\ -e_w U_{\alpha 2} \\ U_{\alpha 3} \end{pmatrix}_{i=1} \tag{26}$$

where e_w is the restitution coefficient for collisions between a particle and the wall, and $i = 0$ represents the wall, assumed to be along the second direction in the considered reference frame. Periodic boundary conditions are imposed by enforcing the periodicity on the set of weights and abscissas. As shown elsewhere,[37] it is straightforward to impose partial reflective and Maxwellian boundary conditions using quadrature-based moment methods.

NUMERICAL SIMULATIONS

The model presented above has been implemented in the CFD code MFIX[57,58] as described in detail elsewhere,[31] and is validated here against the experimental measurements in a gas-particle flow riser with monodisperse[29] and bidisperse particles.[22] Here, we briefly describe the solution procedure and the simulation setup for the mono- and bidisperse cases.

Numerical Solution Procedure. The general procedure for the numerical solution of the moment transport equations and their coupling with the fluid phase is described in detail elsewhere.[31] The fluid-phase equations are solved with an iterative procedure based on the SIMPLE algorithm[59,60] and coupled with the QMOM equations using the partial elimination algorithm.[61] The second-order scheme with a Superbee limiter was used to discretize the fluid-phase equations. The only major difference in comparison to the original algorithm[31] is represented by the treatment of the Boltzmann collision operator because the moments are updated using a numerical time integration rather than using analytical integration, as in the case of the BGK collision model. The effect of collisions on the set of moments is included by solving an ordinary differential equation using operator splitting[31]

$$\frac{\mathrm{d}\mathbf{M}_i}{\mathrm{d}t} = \mathbf{C}_{ij} \tag{27}$$

with a simple Euler method, which leads to

$$\mathbf{M}_i^{(n+1)} = \mathbf{M}_i^{(n)} + \Delta t \mathbf{C}_{ij} \tag{28}$$

where $\mathbf{C}_{ij}$ is the source term given by the quadrature approximation of the moments of the Boltzmann collision integral, and Δt the integration time step, which is limited by a Courant−Friedrichs−Lewy (CFL) condition based on the collision time.

Simulation Setup for Monodisperse Case. The experimental setup[29] is constituted by a riser column of rectangular cross section, as schematically represented in Figure 2. The dimensions of the riser and the properties of the fluid and particle phases are reported in Table 1. The computational domain considered in this work represents only a portion of the whole

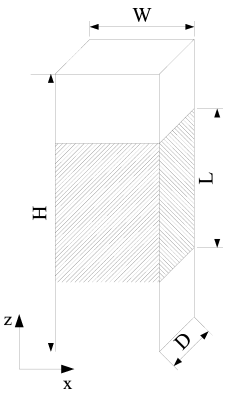

Figure 2. Schematic representation of the riser.[29] Hashed area represents the actual portion of the riser considered in the simulations.

Table 1. Dimensions of Riser and Flow Properties for Monodisperse Case

variable	value	units	variable	value	units
W	0.05	m	H	1.5	m
D	0.015	m	L	0.30	m
d_p	335	μm	ρ_p	2500	kg/m^3
e	0.97	−	G_s	10.0	kg/(m^2 s)
ρ_g	1.2	kg/m^3	μ_g	1.8×10^{-5}	Pa s
U_g	2.3	m/s			

riser examined in the experiments,[29] in the center of the column, with a height L, as represented by the hashed volume in Figure 2. Periodic boundary conditions were imposed at the top and bottom of the computational domain, while no-slip conditions were used for the fluid phase at the wall, and reflective conditions with restitution coefficient $e_w = 1$ were used for the particle phase. It is worth noting that the value of the particle-wall restitution coefficient is not found to significantly impact the riser dynamics.[62] The effect of the tangential restitution coefficient was neglected in this study because the particle angular momentum is not accounted for in the present model. Additionally, it was shown[63,64] that at least for dense flows the effect of the tangential restitution coefficient is negligible for practical values of the wall friction coefficient.

As is customary for simulating fully developed riser flow,[31] the fluid-phase mass flux has been imposed to match the mean particle mass flux G_s by adapting the pressure gradient along the height of the computational domain. We underline that the fully developed riser flow adopted in our simulations only allows a qualitative comparison of the results with the data from the literature because it is apparent[29,30,53] that the simulations used as reference were performed without assuming the domain to be periodic (i.e., the flow statistics are changing in the vertical direction). As will be shown later, the fact that the riser flow is not fully developed in the previous simulations has a significant effect on the flow statistics, particularly in the bidisperse case.

The grid density used in the simulations, taken from the literature,[29] is 25 grid points along W, 60 along L, and 10 along D. A grid-independence study involving simulations of gas-particle flows in a vertical channel with QMOM was performed in our previous work,[65] where we have shown that QBMM allows grid independence to be achieved without the formation of structures at high particle volume fraction whose size is strictly related to the grid size. Simulations were performed with an adaptive time stepping, based on the convergence of the fluid-phase residuals,[57]

dx.doi.org/10.1021/ie300424m | Ind. Eng. Chem. Res. 2013, 52, 187−198

on the QMOM CFL condition on the particle collision time and the drag time. Simulations are carried out for a total of 10 s of simulation time, while time averages are computed on the last 5 s of simulation time. Because the domain is periodic, volume-fraction-weighted averages are computed assuming the z direction to be statistically homogeneous and, considering a symmetry plane located at $W/2$, normal to the x direction. The rms values are found by subtracting the time-average values from the instantaneous fields and time averaging the square of the differences. The final rms values are then the square root of time-average square differences. As discussed elsewhere,[53] the rms values found in this manner are expected to be much larger than those found using the granular temperature.

Simulation Setup for Bidisperse Case. A riser flow used previously in experiments,[22] Euler−Lagrange[30] or Euler−Euler[53] simulations, was used here for testing our simulation code for bidisperse gas-particle flows. The original system has an internal diameter of 0.032 m and is 1.0 m tall. The main properties of the system and of the phases are reported in Table 2. The system is represented in this work by a two-dimensional channel with two parallel walls, consistent with previous simulations[30,53] wherein comparisons between two- and three-dimensional simulations showed no important differences. It is worth noting that only a portion of the system was simulated for a total height of the computational domain equal to 0.3 m. The same numerical configuration (i.e., fully developed riser flow) described above for monodisperse particles with a computational grid of 50 × 120 cells[30] was adopted for bidisperse particles.

Table 2. Dimensions of Riser[22] and Flow Properties for Bidisperse Case

variable	value	units	variable	value	units
D	0.032	m	H	1	m
$d_{p,1}$	120	μm	$d_{p,2}$	185	μm
$\alpha_{p,avg,1}$	0.015	–	$\alpha_{p,avg,2}$	0.015	–
e	0.97	–	ρ_g	1.2	kg/m^3
ρ_p	2400	kg/m^3	μ_g	1.8×10^{-5}	Pa s
U_g	1.0	m/s			

RESULTS AND DISCUSSION

Monodisperse Case. An example of the instantaneous particle volume fraction field at $t = 8$ s obtained in the simulation performed using the quadrature-based moment method is reported in Figure 3a. It is shown that particles segregate at the walls of the riser, forming "packets" at higher volume fraction, which tend to move downward because their weight wins over the resistance exerted by the fluid. As explained elsewhere,[31] the flow evolves from the uniform initial conditions through an intermediate state where particles, due to the reflective conditions at the walls, form two vertical stripes parallel to the walls, with lower particle concentration. In these stripes the fluid accelerates, and the difference in shear causes the flow to become unstable. The instability quickly propagates to the whole flow, leading to the segregation of particles typically observed in turbulent riser flows. The time-average particle volume fraction, shown in Figure 3b (experimental data are not available for this quantity), is lowest in the center of the flow and highest at the walls, which is typical of core-annular flow. As in other gas-particle flows with strong momentum coupling between the phases, the time-average horizontal statistics are mainly determined by the turbulent fluxes and not the particle-phase viscosity and conductivity.

Results of the time-average particle velocity obtained in the simulation performed using QBMM are reported in Figure 4 and compared with the experiments[29] at $z = 0.4$ m. In all the reported plots, $x = 0$ represents the channel centerline, and $x = 0.025$ m

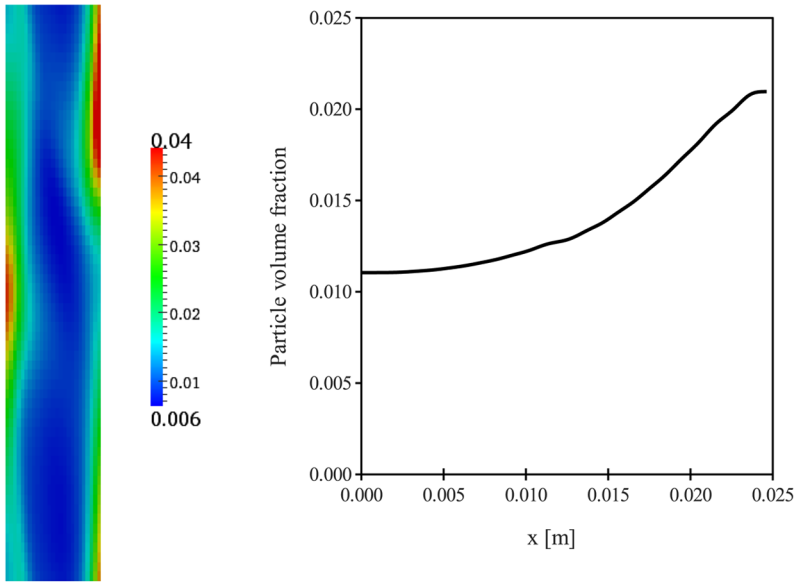

(a) Instantaneous field at $t = 8$ s across the centerline ($D/2$).

(b) Time-average profile.

Figure 3. Particle volume fraction for monodisperse case.

dx.doi.org/10.1021/ie300424m | Ind. Eng. Chem. Res. 2013, 52, 187−198

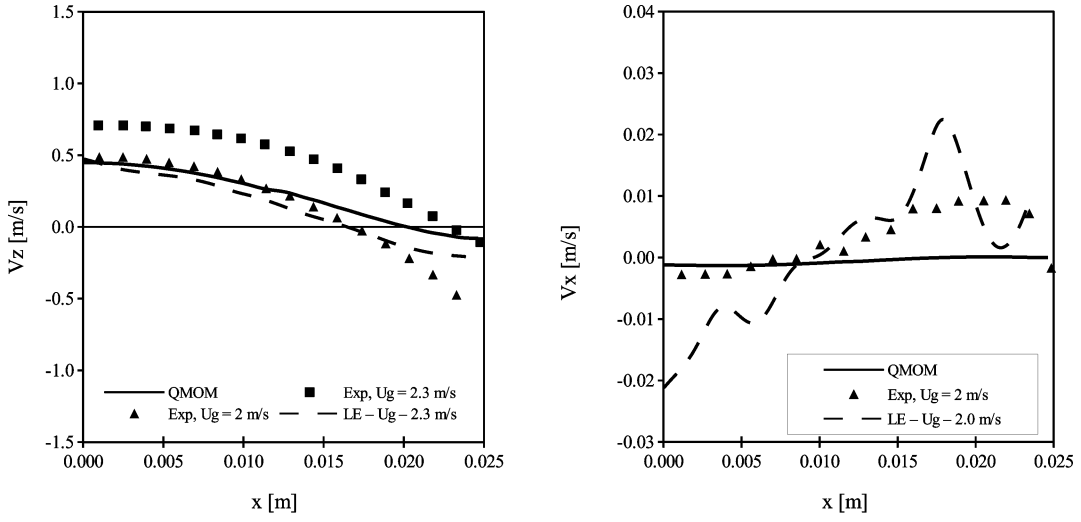

(a) z component (b) x component

Figure 4. Time-average particle velocity for monodisperse case.

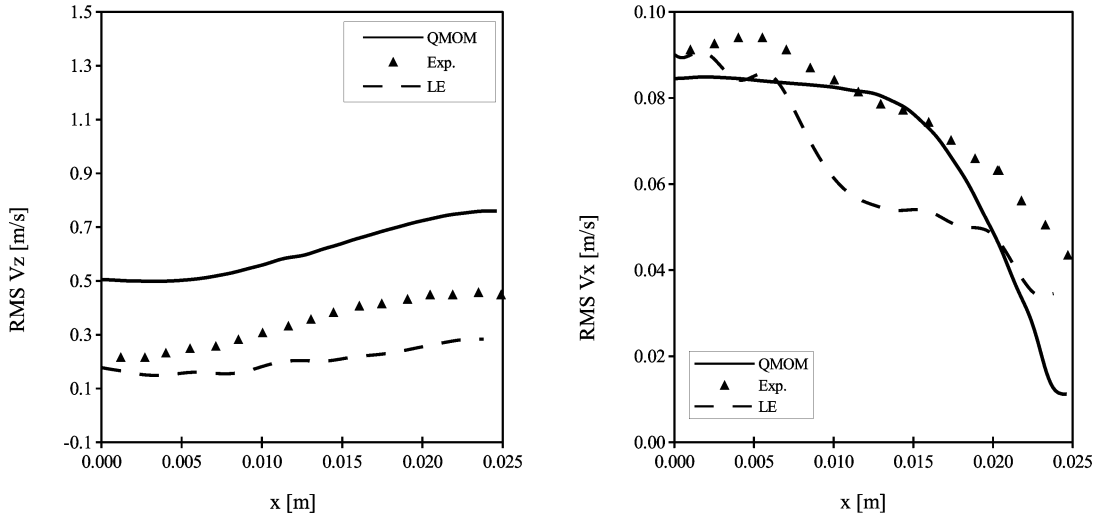

(a) z component (b) x component

Figure 5. Rms particle velocity for monodisperse case.

indicates the channel wall. The predicted values of the vertical velocity (Figure 4a) show a core-annular behavior with negative values at the wall, indicating particles fall in that region of the system and positive values in the center of the riser. Results are in acceptable agreement with the experimental measurements[29] and similar to those obtained by simulations.[29] The convergence of the averages is considered satisfactory, in spite of the relatively short averaging time, because the values of the time-average velocity along the x direction (Figure 4b) are approximately zero, as expected when the flow is fully developed.

The root-mean-square (rms) of the particle velocity is reported in Figure 5 and is in qualitative agreement with the experiments[29] but not in quantitative agreement. For the z component, both the experimental and the computational profiles show a minimum at the riser centerline (Figure 5a) and the maximum value in proximity of the wall but at a certain distance from it. The rms velocity in the x direction, reported in Figure 5(b), is in quantitative agreement with the experimental data. Differences in the numerical predictions compared to the experimental data might depend on the fully developed flow conditions in the QMOM simulation, as opposed to the developing flow in the experiments. Further reasons that could explain the differences are the choice of the drag law, as well as other sub-models used in the numerical model and the systematic errors in the experimental measurements.[29]

The time-average granular temperature is reported in Figure 6. Note that the granular temperature is not the same thing as the rms velocity statistics.[53] The values of Θ_p present a minimum at the wall of the channel, where the collision frequency is higher due to higher particle concentration and to particle segregation, and a maximum in the core of the riser, where the flow is dilute and collisions are not dominant, as shown in Figure 7b. Data for the granular temperature are not available from the experiments or from the Euler−Lagrange simulations for comparison. Nevertheless, as shown by comparing Figure 6 to Figure 5, the

dx.doi.org/10.1021/ie300424m | Ind. Eng. Chem. Res. 2013, 52, 187−198

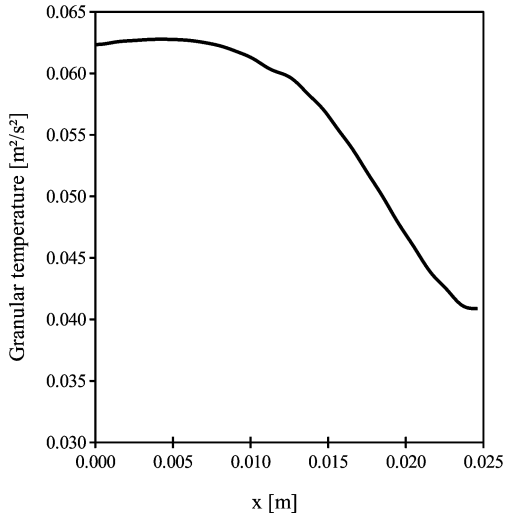

Figure 6. Time-average granular temperature profile for monodisperse case.

square root of the granular temperature is much smaller than the rms particle velocity.

In order to better understand the flow conditions, time-average particle-phase dimensionless numbers are reported in Figure 7. Before proceeding to consider the behavior of the particle Knudsen number, it is worth noting that the particle flow is in transonic conditions, meaning that there are parts of the computational domain where the particle velocity is above or equal to the local particle-phase "speed of sound" (Ma > 1) and other parts of the system where the particle velocity is below the local value of the speed of sound (Ma < 1). This is evident from the values of the time-average local particle Mach number (the instantaneous particle Mach number is defined by $\mathrm{Ma} = |\mathbf{U}_p|/\Theta_p^{1/2}$) in Figure 7a, which shows that the time-average value of Ma is approximately between 6×10^{-3} and 1.8. Under these conditions, two regimes are present in the system. When Ma < 1, the particle-scale fluxes are dominated by diffusive processes, regulated by the local value of the granular temperature, which has to be used to compute the characteristic velocity in this regime. When Ma > 1, the particle-scale fluxes are dominated by convective phenomena, meaning that the transport of properties is mainly due to the convective transport of particles more than to diffusive phenomena, and the granular temperature has to be replaced by the local mean velocity magnitude in the definition of the characteristic velocity of the particle flow. The two zones are separated by a dashed line in Figure 7a.

Because the particle flow undergoes a transition between two different regimes, the definition of the (instantaneous) particle Knudsen number has to be modified according to the region where it is computed[66]

$$\mathrm{Kn} = \begin{cases} \sqrt{\frac{\pi}{2}}\frac{\tau_c \Theta_p^{1/2}}{L} & \mathrm{Ma} < 1 \\ \sqrt{\frac{\pi}{2}}\frac{\tau_c |\mathbf{U}_p|}{L} & \mathrm{Ma} > 1 \end{cases} \tag{29}$$

where the collision time is given by

$$\tau_c = \frac{d_p}{12 g_0 \alpha_p}\sqrt{\frac{\pi}{\Theta_p}} \tag{30}$$

The values of the time-average particle Knudsen number, computed assuming $L = 2WD/(W + D)$, according to the definition of hydraulic diameter of the riser, are reported in Figure 7b. The diagram shows the flow transitions from the slip regime,[67] where 0.01 < Kn < 0.1, in the region adjacent to the wall, to a more rarefied regime (*transitional* regime) in the center of the riser, where nonequilibrium phenomena are expected to happen. The two regions are separated by the dotted line in Figure 7b. The lower value of Kn at the wall is justified by the higher particle concentration in that region of the system, which leads to higher values of the collision frequency, making the flow locally dominated by collisions. It is worth noting that if a hydrodynamic model,[41,42,53] derived with the hypothesis of small particle Knudsen number (continuum regime, Kn < 0.01), were used to perform the simulations, the adoption of partial slip boundary conditions[68] would have been necessary to describe the behavior of the particle flow in the zone adjacent to the walls, where Kn ≈ 0.1. However, the hydrodynamic model may deviate from the correct behavior in the center of the riser, where higher values of the particle Knudsen number are present.

The time-average particle Stokes number profile is reported in Figure 7c and exhibits values between 66 and 124, which indicate that a particle's response to changes in the local conditions of the fluid flow is not instantaneous but delayed, and because the

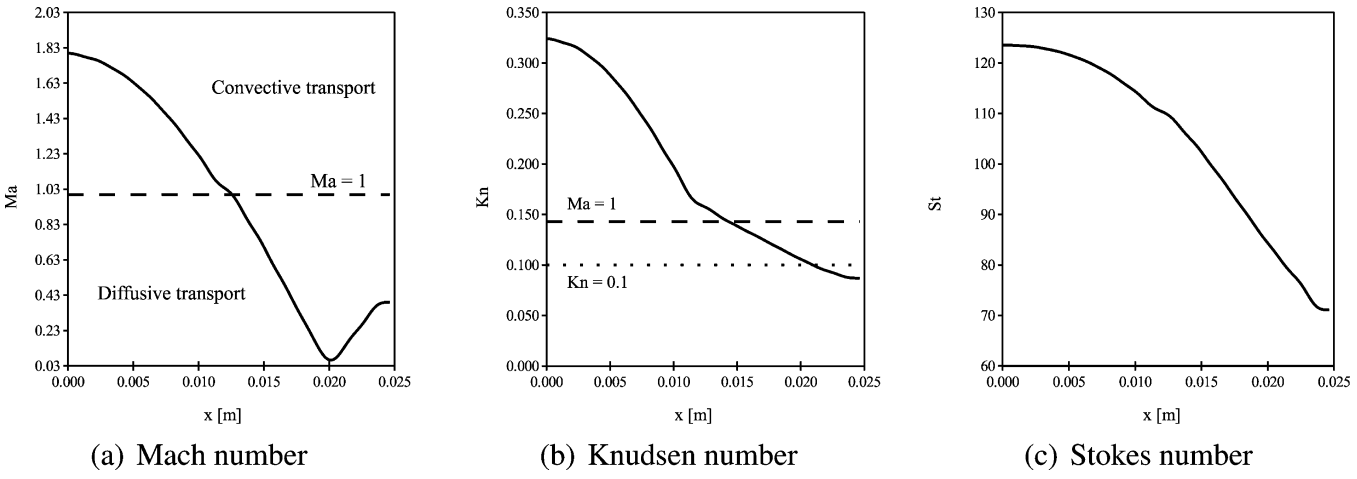

Figure 7. Time-average particle-phase dimensionless numbers for monodisperse case.

dx.doi.org/10.1021/ie300424m | *Ind. Eng. Chem. Res.* 2013, 52, 187−198

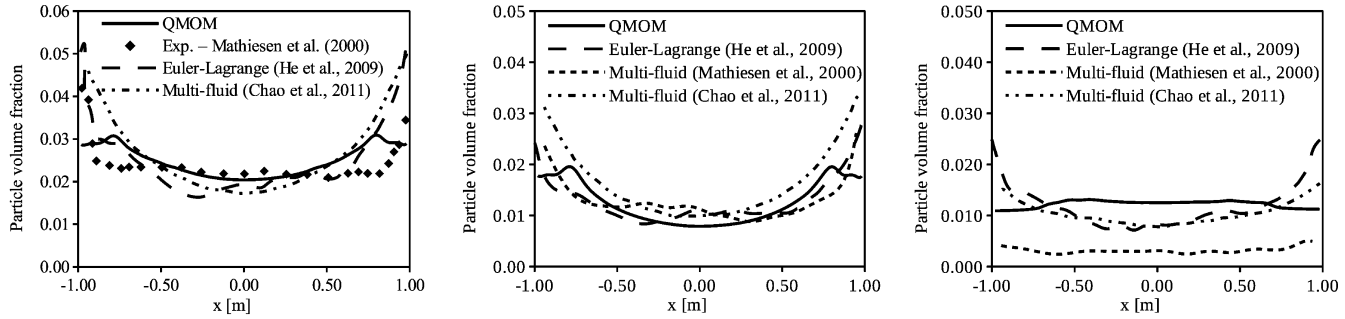

(a) Total volume fraction ($\alpha_{p,1}+\alpha_{p,2}$) (b) $d_p = 120\ \mu m$ (c) $d_p = 185\ \mu m$

Figure 8. Time-average particle volume fraction for bidisperse case.

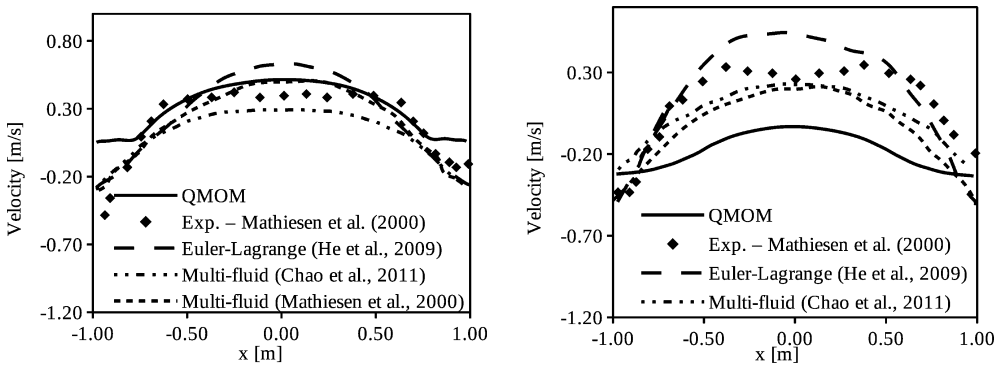

(a) $d_p = 120\ \mu m$ (b) $d_p = 185\ \mu m$

Figure 9. Time-average vertical particle velocity for bidisperse case.

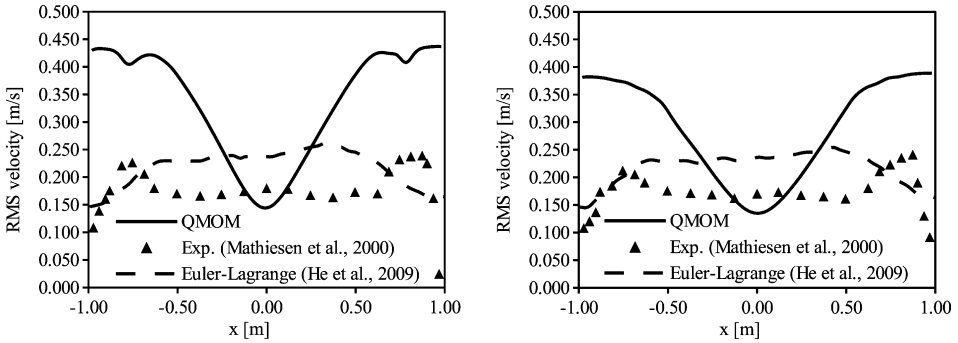

(a) $d_p = 120\ \mu m$ (b) $d_p = 185\ \mu m$

Figure 10. Streamwise rms particle velocity for bidisperse case.

particle flow is relatively dilute, it could lead to particle trajectory crossing. As pointed out elsewhere,[34] such phenomenon cannot be accurately predicted by hydrodynamic models because they only consider moments up to second order and define only one local velocity in each computational cell, whereas multiple local velocities are necessary to be able to capture the discontinuous particle velocity field that originates from particle trajectory crossing. Nevertheless, as indicated by the particle Knudsen number less than unity in Figure 7b, particle−particle collisions in the monodisperse case are frequent enough to substantially smooth out the effects of particle trajectory crossing in the monodisperse case.

Bidisperse Case. The time-average profile of the total particle volume fraction ($\alpha_{p,1} + \alpha_{p,2}$) is reported in Figure 8a and compared with experimental measurements[22] at z = 0.4 m, the Euler−Lagrange simulations,[30] and multi-fluid simulations.[22,53] The profile is characterized by a qualitative prediction of the total particle concentration in the center of the channel and shows the typical structure of core-annular flow. However, the value of the particle volume fraction at the walls is underestimated, and thus, the thickness of the annulus is overestimated in the QMOM simulation. The QMOM simulation predicted the volume fraction profile of the smallest particles present in the system (d_p = 120 μm) in fair agreement with the Euler−Lagrange simulations,[30] as shown in Figure 8b. However, the profile obtained with QMOM is more symmetric, perhaps due to the absence of statistical noise caused by having a finite number of particles in the Euler−Lagrange simulations, and exhibits less segregation near the walls. On the other hand, the segregation of the largest particles (d_p = 185 μm) has the same average value as

dx.doi.org/10.1021/ie300424m | Ind. Eng. Chem. Res. 2013, 52, 187−198

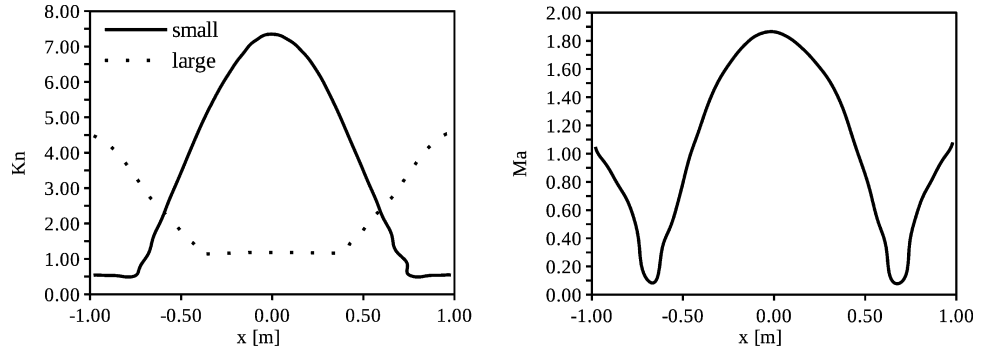

(a) Kn (b) Ma

Figure 11. Time-average profiles of (a) Knudsen number for each species and (b) Mach number of the mixture.

the Euler−Lagrange simulation (Figure 8c), but the QMOM concentration profile of these particles is nearly flat, while the Euler−Lagrange simulation exhibits significant accumulation at the walls. The QMOM profile qualitatively resembles the ones reported in the literature[22,53] for the same case using multi-fluid simulations. However, the average value is different due to the fully developed flow conditions used in the QMOM simulation.

The vertical velocity of particles with $d_p = 120\ \mu m$ is predicted in fair agreement with the experimental measurements, as shown in Figure 9a. However, the maximum axial velocity is underestimated with respect to its experimental value, and particle downfall along the walls is not properly captured. The predicted vertical velocity of larger particles shown in Figure 9b is significantly underestimated with respect to both the Euler−Lagrange and experimental results. This difference is due to the fully developed flow conditions used in the QMOM simulation as compared to the developing flow conditions used in He et al.[30] Indeed, for the fully developed flow we observe that the average vertical velocity of the larger particles is negative, indicating that the large particles would not be able to exit the top of a sufficiently high riser for the pressure drop used in the QMOM simulations.

The profiles of the streamwise rms velocities of the two particle types are reported in Figure 10. For both particle types, the profile of the rms velocity is larger than in the experiments and Euler−Lagrange simulations, except at the center of the domain where the agreement is satisfactory. The large difference near the walls is likely due to the fully developed flow adopted in the QMOM simulations. As shown in Figure 9, this results in a larger difference between the time-average vertical particle velocities, which leads to larger rms velocities due to collisions between particles of different types.

We now examine the particle Knudsen and the Mach number in the bidisperse system, as done for the monodisperse case. The Knudsen number is computed for each species independently, following eq 29. However, the definition of the particle Mach number has to be extended to a mixture of particle types. We adopt here a definition based on the ratio of the velocity of the granular mixture and the square root of the granular temperature of the mixture

$$\mathrm{Ma} = \frac{|\mathbf{U}_{\mathrm{mix}}|}{\sqrt{\Theta_{\mathrm{mix}}}}$$

where

$$\mathbf{U}_{\mathrm{mix}} = \frac{\alpha_{\mathrm{p},1}\mathbf{U}_{\mathrm{p},1} + \alpha_{\mathrm{p},2}\mathbf{U}_{\mathrm{p},2}}{\alpha_{\mathrm{p},1} + \alpha_{\mathrm{p},2}}$$

and

$$\Theta_{\mathrm{mix}} = \frac{\alpha_{\mathrm{p},1}\Theta_{\mathrm{p},1} + \alpha_{\mathrm{p},2}\Theta_{\mathrm{p},2}}{\alpha_{\mathrm{p},1} + \alpha_{\mathrm{p},2}}$$

Figure 11a shows the time-average values of the Knudsen number for each species, which clearly demonstrate that the fully developed riser flow is not collision dominated. It is worth noting that the reported values do not account for collisions between different particle types. However, it is reasonable to assume that such an effect would not change the order of magnitude of the Knudsen numbers. The time-average value of the particle Mach number reported in Figure 11b is always above one in the center of the channel, indicating that the flow is dominated by convective transport of momentum rather than by collisional transport. For such flow conditions, polydisperse kinetic theories using the Chapman−Enskog expansion to close the collision integral can not be justified because they are derived with the assumption that the particle Knudsen numbers are small. High-order moment methods with quadrature closures, on the other hand, are not affected by this restriction.[45,69]

CONCLUSIONS

A fully developed riser flow, representing a portion of a circulating fluidized bed, has been simulated using a third-order QBMM. The simulations demonstrate the robustness and the capability of QBMM for simulating dilute mono- and bidisperse gas-particles flows. Results for the time-average particle velocity were found to be in reasonable agreement with the experimental results for developing flow in a riser. rms velocities for the streamwise component were also found to be in qualitative agreement with experiments. Furthermore, the simulation results for the bidisperse case demonstrate for the first time the applicability of the quadrature-based closure of the full Boltzmann collision integral in eq 25 for gas-particle flows.

Characteristic dimensionless numbers of the particle flow were examined for the monodisperse case. The value of the particle Knudsen number demonstrates that the flow is in a condition spanning two regimes: the slip regime (zone adjacent to the wall) and the transition regime (center of the channel), indicating that the adoption of hydrodynamic models for this flow would be inappropriate. High-order moment methods, on the contrary, are better suited to account for finite-Knudsen effects.[37] The particle Mach number showed that the particle phase is in transonic

dx.doi.org/10.1021/ie300424m | Ind. Eng. Chem. Res. 2013, 52, 187−198

conditions, with a subsonic region adjacent to the wall. This was further confirmed by considering the local values of the particle Stokes number, which clarified that particles do not immediately react to the fluid flow.

For the bidisperse case, the values of the particle Knudsen number indicate that momentum transport is not dominated by collisions, justifying the adoption of high-order moment methods, not constrained by the hydrodynamic limit assumption, also for this case. Nonetheless, because momentum coupling between the phases in both cases generates strongly time-dependent turbulent flow, the exact formulation of the microscale transport equations may turn out to be less important than the models for turbulent fluxes needed to close the Favre-average transport equations.[1] Indeed, the computational cost of fully resolving even the simplest multiphase hydrodynamic model (i.e., inviscid flow for both phases) puts the simulation of industrial equipment beyond reach without a predictive multiphase turbulence model.[70]

Future work with QBMM will involve the simulation of systems with more realistic boundary conditions (e.g., rough walls) and geometries than those considered in the present work. Further work is also needed to develop turbulence models in the context of QBMM[1] that properly account for the momentum coupling and its role in generating two-phase turbulence.

AUTHOR INFORMATION

Corresponding Author

*E-mail: albertop@iastate.edu (A.P.); rofox@iastate.edu (R.O.F.).

Notes

The authors declare no competing financial interest.

ACKNOWLEDGMENTS

This work has been supported by the National Energy Technology Laboratory of the U.S. Department of Energy under Award Number DE-FC26-07NT43098.

REFERENCES

(1) Fox, R. O. Large-eddy-simulation tools for multiphase flows. *Annu. Rev. Fluid Mech.* **2012**, *44*, 47−76.

(2) Syamlal, M.; Gidaspow, D. Hydrodynamics of fluidization: Prediction of wall to bed heat transfer coefficient. *AIChE J.* **1985**, *31*, 127−135.

(3) Gidaspow, D. Hydrodynamics of fluidization and heat transfer: Supercomputer modeling. *Appl. Mech. Rev.* **1986**, *39*, 1−22.

(4) Wen, C. Y.; Yu, Y. H. Mechanics of fluidization. *Chem. Eng. Prog., Symp. Ser.* **1966**, *62*, 100−111.

(5) Gidaspow, D.; Tsuo, Y. P.; Luo, K. M. In *Fluidization IV*; Grace, J. C., Schemilt, L. W., Sun, G., Eds.; Engineering Foundation: New York, 1989; pp 81 − 88.

(6) Tsuo, Y. P.; Gidaspow, D. Computation of flow patterns in circulating fluidized beds. *AIChE J.* **1990**, *86*, 886−896.

(7) Sinclair, J. L.; Jackson, R. Gas-particle flow in a vertical pipe with particle-particle interaction. *AIChE J.* **1989**, *35*, 1473−1486.

(8) Sinclair, J. L. In *Circulating Fluidized Beds*, 1st ed.; Grace, J. R., Avidan, A. A., Knowlton, T. M., Eds.; Blackie Academic & Professional: London, 1997; Chapter 5, pp 149−180.

(9) Pita, J. A.; Sundaresan, S. Gas-solid flow in vertical tubes. *AIChE J.* **1991**, *37*, 1009−1018.

(10) Bader, R.; Findlay, J.; Knowlton, T. In *Circulating Fluidized Bed Technology II*; Basu, P., Large, J. F., Eds.; Pergamon Press: New York, 1988; pp 123 − 137.

(11) Lounge, M.; Mastorakos, E.; Jenkins, J. T. The role of particle collision in pneumatic transport. *J. Fluid Mech.* **1991**, *231*, 345−359.

(12) Gidaspow, D.; Therdthianwong, A. In *Circulating Fluidized Bed Technology IV*; Avidan, A. A., Ed.; AIChE: New York, 1993; pp 32 − 39.

(13) Ocone, R.; Sundaresan, S.; Jackson, R. Gas-particle flow in a duct of arbitrary inclination with particle-particle interactions. *AIChE J.* **1993**, *39*, 1261−1271.

(14) Bolio, E. J.; Yasuna, J. A.; Sinclair, J. L. Dilute turbulent gas-solid flow with particle−particle interaction. *AIChE J.* **1995**, *41*, 1375−1388.

(15) Hrenya, C. M.; Sinclair, J. L. Effects of particle-phase turbulence in gas−solid flows. *AIChE J.* **1997**, *43*, 853−869.

(16) Benyahia, S.; Arastoopour, H.; Knowlton, T. M.; Massah, H. Simulation of particles and gas flow behavior in the riser section of a circulating fluidized bed using the kinetic theory approach for the particulate phase. *Powder Technol.* **2000**, *112*, 24−33.

(17) Arastoopour, H. Numerical simulation and experimental analysis of gas/solid flow systems: 1999 Fluor-Daniel plenary lecture. *Powder Technol.* **2001**, *119*, 59−67.

(18) Peirano, E.; Leckner, B. Fundamentals of turbulent gas−solid flows applied to circulating fluidized bed combustion. *Prog. Energy Combust. Sci.* **1998**, *24*, 259−296.

(19) Peirano, E.; Delloume, V.; Johnsson, F.; Leckner, B.; Simonin, O. Numerical simulation of the fluid dynamics of a freely bubbling fludized bed: Influence of the air supply system. *Powder Technol.* **2002**, *122*, 69−82.

(20) DeWilde, J.; Heynderickx, G. J.; Vierendeels, J.; Dick, E.; Marin, G. B. An extension of the preconditioned advection upstream splitting method for 3D two-phase flow calculations in circulating fluidized beds. *Comput. Chem. Eng.* **2002**, *26*, 1677−1702.

(21) Samuelsberg, A.; Hjertager, B. H. An experimental and numerical study of flow patterns in a circulating fluidized bed reactor. *Int. J. Multiphase Flow* **1996**, *22*, 575−591.

(22) Mathiesen, V.; Solberg, T.; Hjertager, B. H. An experimental and computational study of multiphase flow behavior in a circulating fluidized bed. *Int. J. Multiphase Flow* **2000**, 387−419.

(23) Lu, H.; Gidaspow, D. Hydrodynamics of binary fluidization in a riser: CFD simulation using two granular temperatures. *Chem. Engng. Sci.* **2003**, *58*, 3777−3792.

(24) Lu, H.; Yunhua, Z.; Zhiheng, S.; Ding, J.; Juying, J. Numerical simulation of gas−solid flow in tapered risers. *Powder Technol.* **2006**, *169*, 89−98.

(25) Smagorinsky, J. General circulation experiments with the primitive equations. *Mon. Weather Rev.* **1963**, *91*, 99−164.

(26) Ibsen, C. H.; Helland, E.; Hjertager, B. H.; Solberg, T.; Tadrist, L.; Occelli, R. Comparison of multi-fluid and discrete particle modelling in numerical predictions of gas particle flow in circulating fluidised beds. *Powder Technol.* **2004**, *149*, 29−41.

(27) Zeng, Z. X.; Zhou, L. X. A two-scale second-order moment particle turbulence model and simulation of dense gas-particle flows in a riser. *Powder Technol.* **2006**, *162*, 27−32.

(28) Moreau, M.; Simonin, O.; Bedat, B. Development of gas-particle Euler−Euler LES approach: a priori analysis of particle sub-grid models in homogeneous isotropic turbulence. *Flow Turbul. Combust.* **2009**, *84*, 295−324.

(29) He, Y.; Deen, N.; Van Sint Annaland, M.; Kuipers, J. A. M. Gas-solid turbulent flow in a circulating fluidized bed riser: Experimental and numerical study of monodisperse particle systems. *Ind. Eng. Chem. Res.* **2009**, 8091−8097.

(30) He, Y.; Deen, N.; Van Sint Annaland, M.; Kuipers, J. A. M. Gas-solid turbulent flow in a circulating fluidized bed riser: Numerical study of binary particle systems. *Ind. Eng. Chem. Res.* **2009**, 8098−8108.

(31) Passalacqua, A.; Fox, R. O.; Garg, R.; Subramaniam, S. A fully coupled quadrature-based moment method for dilute to moderately dilute fluid-particle flows. *Chem. Eng. Sci.* **2010**, *65*, 2267−2283.

(32) Fox, R. O.; Vedula, P. Quadrature-based moment model for moderately dense polydisperse gas-particle flows. *Ind. Eng. Chem. Res.* **2010**, *49*, 5174−5187.

(33) Marchisio, D. L.; Fox, R. O. Implementation of the quadrature method of moments in CFD codes for aggregation-breakage problems. *Chem. Eng. Sci.* **2003**, *58*, 3337−3351.

(34) Desjardin, O.; Fox, R. O.; Villedieu, P. A quadrature-based moment method for dilute fluidparticle flows. *J. Comput. Phys.* **2008**, *227*, 2524−2539.
(35) Fox, R. O. A quadrature-based third-order moment method for dilute gas-particle flows. *J. Comput. Phys.* **2008**, *227*, 6313−6350.
(36) Fox, R. O. Higher-order quadrature-based moment methods for kinetic equations. *J. Comput. Phys.* **2009**, *228*, 7771−7791.
(37) Passalacqua, A.; Galvin, J. E.; Vedula, P.; Hrenya, C. M.; Fox, R. O. A quadrature-based kinetic model for dilute non-isothermal granular flows. *Commun. Comput. Phys.* **2011**, *10*, 216−252.
(38) Vikas, V.; Wang, Z. J.; Passalacqua, A.; Fox, R. O. Realizable high-order finite-volume schemes for quadrature-based moment methods. *J. Comput. Phys.* **2011**, *230*, 5328−5352.
(39) Yuan, C.; Fox, R. O. Conditional quadrature method of moments for kinetic equations. *J. Comput. Phys.* **2011**, *230*, 8216−8246.
(40) Drew, D. A. Averaged equations for two-phase flows. *Stud. Appl. Math.* **1971**, *L*, 205−231.
(41) Gidaspow, D. *Multiphase Flow and Fluidization*; Academic Press: San Diego, 1994.
(42) Enwald, H.; Peirano, E.; Almstedt, A. E. Eulerian two-phase flow theory applied to fluidization. *Int. J. Multiphase Flow* **1996**, *22*, 21−66.
(43) Chapman, S.; Cowling, T. G. *The Mathematical Theory of Non-Uniform Gases*, 2nd ed.; Cambridge University Press: New York, 1961.
(44) Cercignani, C.; Illner, R.; Pulvirenti, M. *The Mathematical Theory of Dilute Gases*; Springer-Verlag: Berlin, 1994.
(45) Struchtrup, H. *Macroscopic Transport Equations for Rarefied Gas Flows*; Springer: Berlin, 2005.
(46) Perthame, B. Boltzmann type schemes for compressible Euler equations in one and two space dimensions. *SIAM J. Num. Anal.* **1990**, *29*, 1−19.
(47) Cercignani, C. *Theory and Application of the Boltzmann Equation*; Scottish Academic Press: London, 1975.
(48) Cercignani, C. *The Boltzmann Equation and its Applications*; Springer-Verlag: Berlin, 1988.
(49) Bhatnagar, P. L.; Gross, E. P.; Krook, M. A model for collisional processes in gases. I. Small amplitude processes in charged and neutral one-component systems. *Phys. Rev.* **1954**, *94*, 511−525.
(50) Holway, H. L. New statistical models for kinetic theory, methods of construction. *Phys. Fluids* **1966**, *9*, 1658−1673.
(51) Carnahan, N. F.; Starling, K. E. Equation of state for nonattracting rigid spheres. *J. Chem. Phys.* **1969**, *51*, 635−636.
(52) Goldschmidt, M. J. V.; Beetstra, R.; Kuipers, J. A. M. Hydrodynamic modelling of dense gas-fluidised beds: Comparison of the kinetic theory of granular flow with 3D hard-sphere discrete particle simulations. *Chem. Eng. Sci.* **2002**, *57*, 2059−2075.
(53) Chao, Z.; Wang, Y.; Jakobsen, J. P.; Fernandino, M.; Jakobsen, H. A. Derivation and validation of a binary multi-fluid Eulerian model for fluidized beds. *Chem. Eng. Sci.* **2011**, *66*, 3605−3616.
(54) Dahl, S. R.; Hrenya, C. M.; Garzo, V.; Dufty, J. W. Kinetic temperatures for a granular mixture. *Phys. Rev. E* **2002**, *66*, 041301.
(55) Andries, P.; Aoki, K.; Perthame, B. A consistent BGK-type model for gas mixtures. *J. Stat. Phys.* **2002**, *106*, 993−1018.
(56) When the diameter ratio is varied, both the material densities ρ_1 and ρ_2 as well as the number concentrations n_1 and n_2 must be varied to keep the species volume fractions equal.
(57) Syamlal, M.; Rogers, W.; O'Brien, T. J. *MFIX Documentation Theory Guide*. U.S. Department of Energy, Office of Fossil Energy, Morgantown Energy Technology Center: Morgantown, WV, 1993.
(58) Syamlal, M. *MFIX Documentation Numerical Technique*. U.S. Department of Energy, Office of Fossil Energy, Federal Energy Technology Center: Morgantown, WV, 1998.
(59) Patankar, S. *Numerical Heat Transfer and Fluid Flow*; Taylor & Francis: New York, 1980.
(60) Ferziger, J. H.; Peric, M. *Computational Methods for Fluid Dynamics*; Springer-Verlag: Berlin, 2002.
(61) Spalding, D. B. Numerical Computation of Multi-Phase Fluid Flow and Heat Transfer. In *Recent Advances in Numerical Methods in Fluids*, Volume 1; Pineridge Press, Ltd.: Swansea, U.K., 1980; pp 139−167.
(62) Almuttahar, A.; Taghipour, F. Computational fluid dynamics of high density circulating fluidized bed riser: Study of modeling parameters. *Powder Technology* **2008**, *185*, 11−23.
(63) Hoomans, B. P. B. *Granular Dynamics of Gas−Solid Two-Phase Flows*. Ph.D. Thesis, Twente University, Enschede, The Netherlands, 2000.
(64) Goldschmidt, M. J. V.; Kuipers, J. A. M.; van Swaaij, W. P. M. Hydrodynamic modeling of dense gas-fluidised beds using the kinetic theory of granular flow: effect of coefficient of restitution on bed dynamics. *Chem. Eng. Sci.* **2001**, *56*, 571−578.
(65) Passalacqua, A.; Fox, R. O. Advanced continuum modelling of gas-particle flows beyond the hydrodynamic limit. *Appl. Math. Model* **2011**, *35*, 1616−1627.
(66) Kogan, M. N. *Rarified Gas Dynamics*; Plenum Press: New York, 1969.
(67) Bird, G. A. *Molecular Gas Dynamics and the Direct Simulation of Gas Flows*; Oxford University Press: Oxford, U.K., 1994.
(68) Johnson, P. C.; Jackson, R. Frictional-collisional constitutive relations for granular materials, with applications to plane shearing. *J. Fluid Mech.* **1987**, *176*, 67−93.
(69) Grad, H. On the kinetic theory of rarefied gases. *Commun. Pure Appl. Math.* **1949**, *2*, 331−407.
(70) Rao, A.; Curtis, J. S.; Hancock, B. C.; Wassgren, C. Numerical simulation of dilute turbulent gas-particle flow with turbulence modulation. *AIChE J.* **2012**, *58*, 1381−1396.